Electronic Supplementary Information

Construction of Bimetallic Nickel Cobalt Selenides Pompon as Superior Anode for High Performance Sodium Storage

Wei Zhong,† Qianru Ma,† Wenwen Tang, Yuanke Wu, Wei Gao, Qiuju Yang, Shu-Juan Bao, * Maowen Xu*

Institute for Clean Energy and Advanced Materials, Faculty of Materials and Energy, Southwest University, Chongqing 400715, PR China

† These two authors contributed equally to this work.

* E-mail: yjg20140716@swu.edu.cn; xumaowen@swu.edu.cn.

1. Materials Characterizations

The morphology was observed by field emission scanning electron microscopy (FESEM) using JSM-7800F (Japan) with Energy-dispersive spectroscopy (EDS), and the microstructure of the material was analyzed by transmission electron microscopy (TEM) of JEM-2100 (Japan). Cu Kα radiation X-ray diffraction (XRD-7000) with a wavelength of 1.5406 Å was used to exam the crystal structure of the material. The X-ray photoelectron spectroscopy (XPS) of the products were obtained from a Thermo Scientific Escalab 250xi spectrometer. The analysis of pore size and specific surface area was mainly based on Autosorb-1 (Quantachrome Instruments, USA).

2. Electrochemical Measurements

The electrochemical properties of the material are mainly manifested by the CR2032 cells assembled in a glove box filled with Ar. The preparation process of the anode working electrode followed a conventional method. Typically, the active materials, carbon black and polyvinylidene fluoride binder were homogeneously mixed at a mass ratio of 8:1:1 with N-methyl-2-pyrrolidone (NMP) as solvent. Then the obtained slurry was pasted onto a polished and clean Cu foil and transferred to a 120 °C vacuum oven for 12 h to remove the NMP solvent. The mass loading of each electrode slice (12mm diameter) is approximately 1.0 mg cm^{-2}, and the thickness of active material is about 10 μm. The glass fiber and metal sodium slices were employed as the separator and counter electrode, respectively. The injected electrolyte component was 1 mol L-1 sodium trifluoromenthanesulfonate (NaCF3SO3) in diethylene glycol dimethyl ether (DEGDME). The galvanostatic charge/discharge test

was performed by Land battery test system (Wuhan, China) in a voltage window of 0.4 V - 2.9 V at desired current density. The cyclic voltammetry (CV) of the cell at different sweep speeds from 0.1-1.0 mV s-1 was completed by the CHI 660E electrochemical workstation. Zahner electrochemical workstation (Zennium, IM6,Germany) was applied to investigate the electrochemical impedance spectroscopy (EIS).

Supplementary Figures

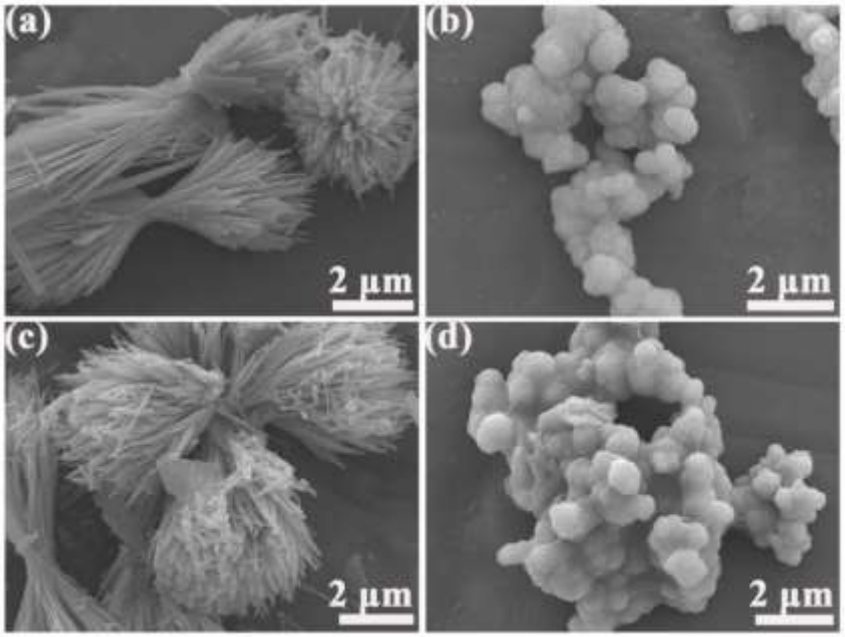

Fig. S1. (a-b) FESEM images of Co and Ni precursor. (c-d) FESEM images of Co_9Se_8 and $Ni_{0.85}Se$ composites.

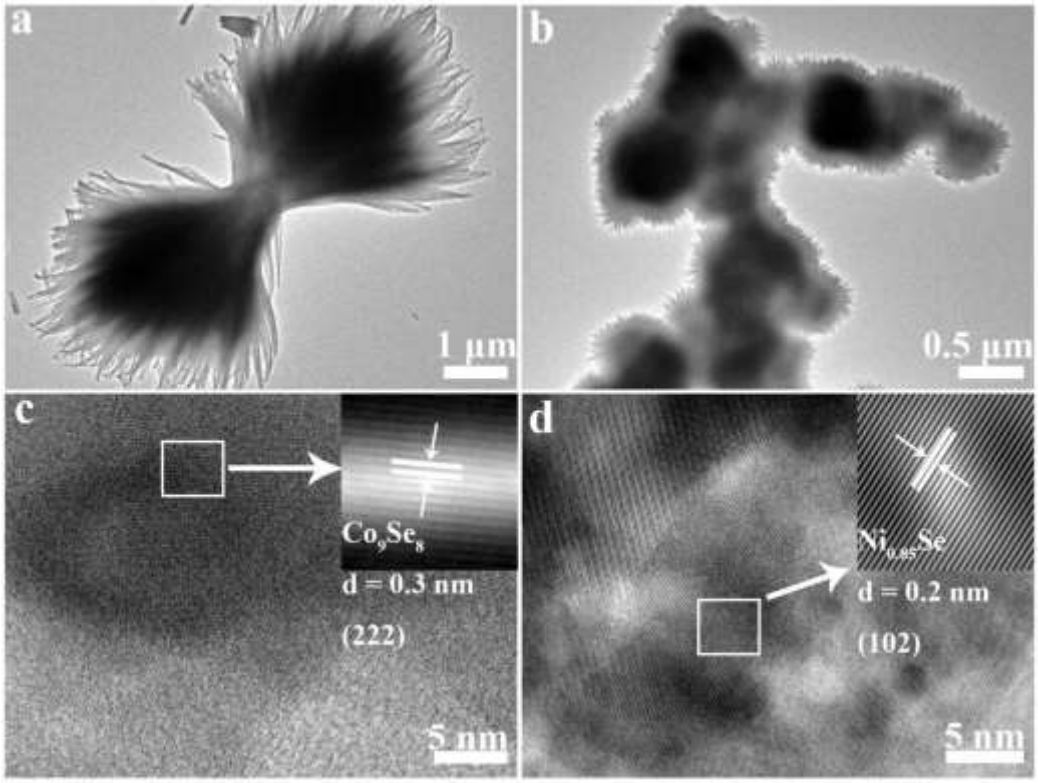

Fig. S2. (a-b) Low-magnification TEM images of Co_9Se_8 and $Ni_{0.85}Se$. (c-d) High-magnification TEM images of Co_9Se_8 and $Ni_{0.85}Se$.

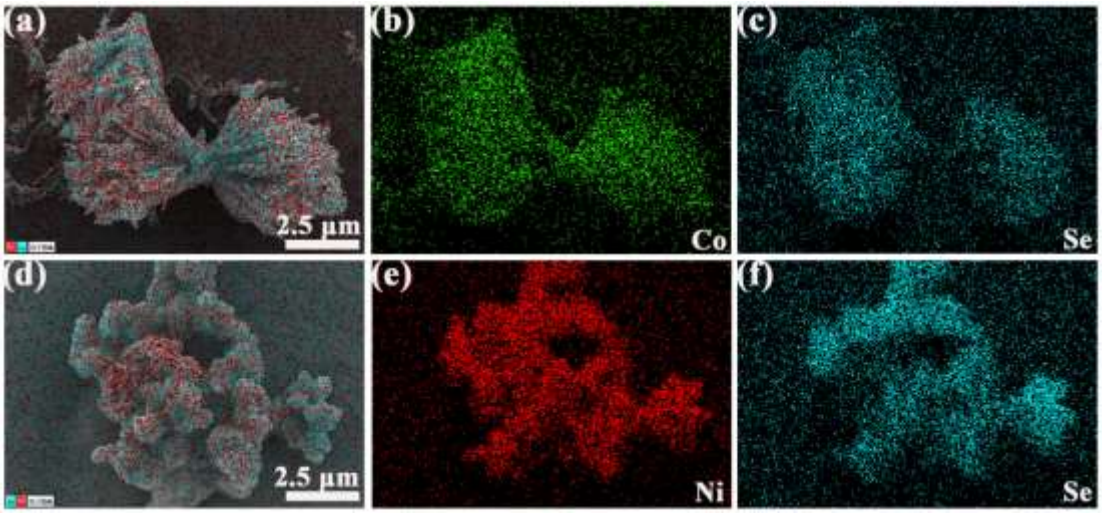

Fig. S3. EDS mapping images of (a-c) Co_9Se_8 and (d-f) $Ni_{0.85}Se$.

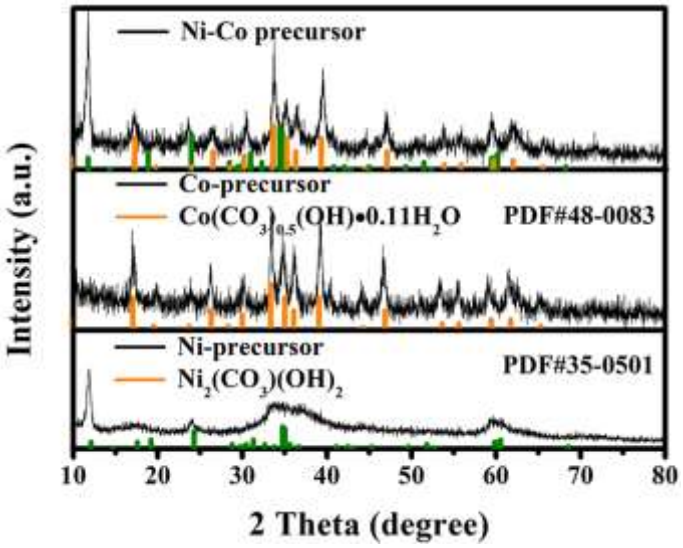

Fig. S4. XRD patterns of Ni-Co, Co and Ni precursor.

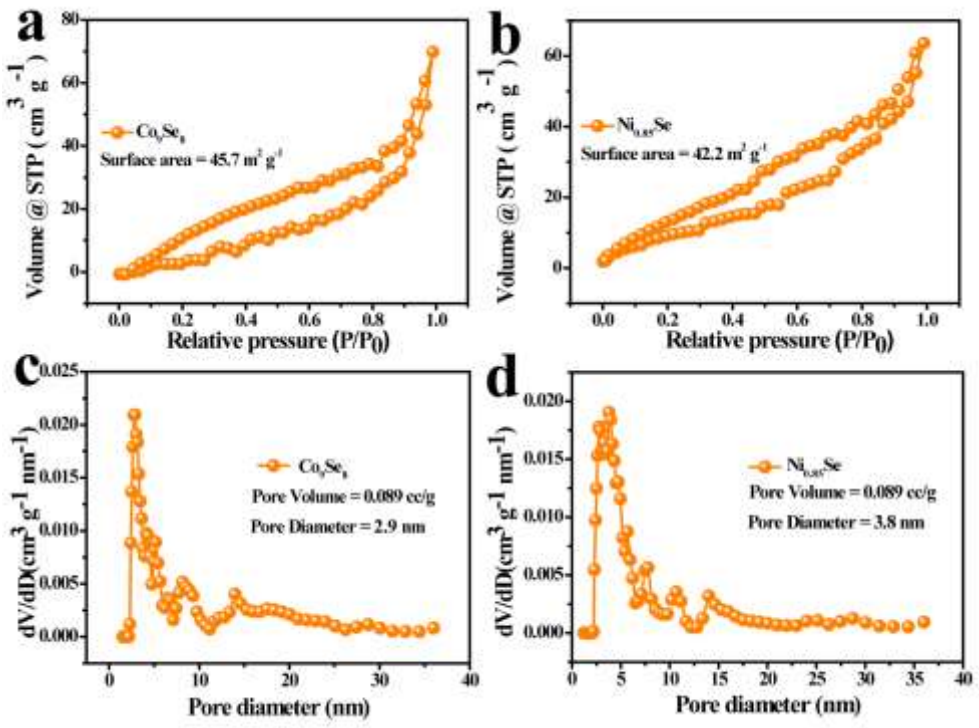

Fig. S5. Nitrogen sorption isotherms of (a) Co_9Se_8 and (b) $Ni_{0.85}Se$. Pore size distribution of (c) Co_9Se_8 and (d) $Ni_{0.85}Se$.

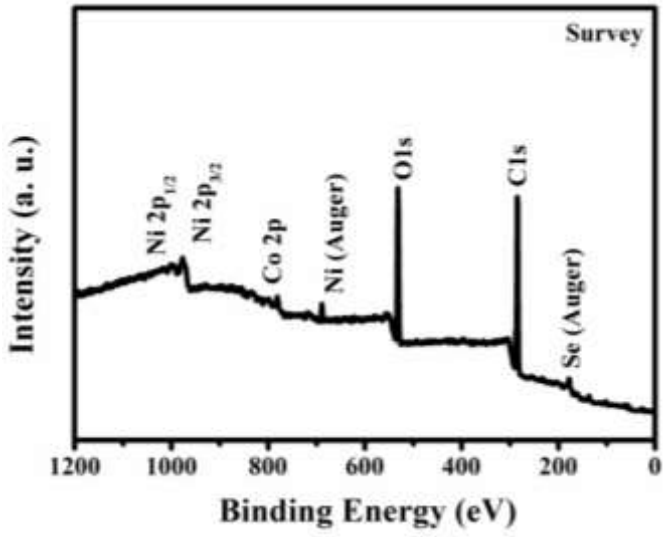

Fig. S6. XPS survey spectrum of $NiCo_2Se_4$.

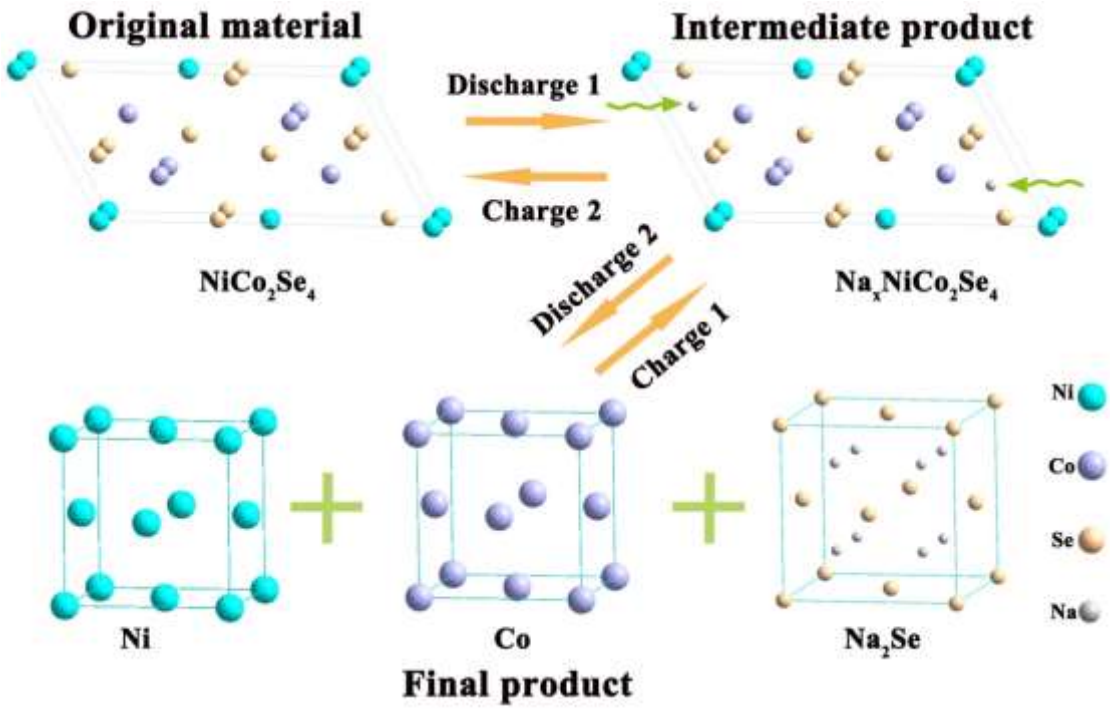

Fig. S7. Charging/discharging mechanism schematic.

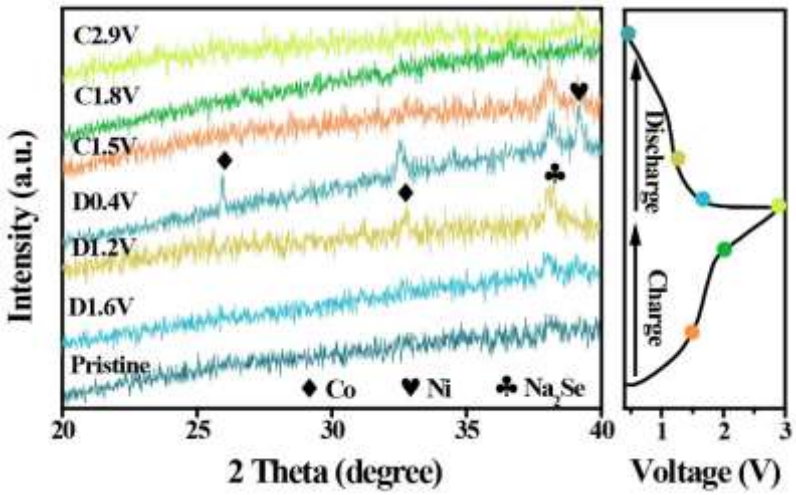

Fig. S8. Ex situ XRD pattern of $NiCo_2Se_4$ electrodes during charge/discharge.

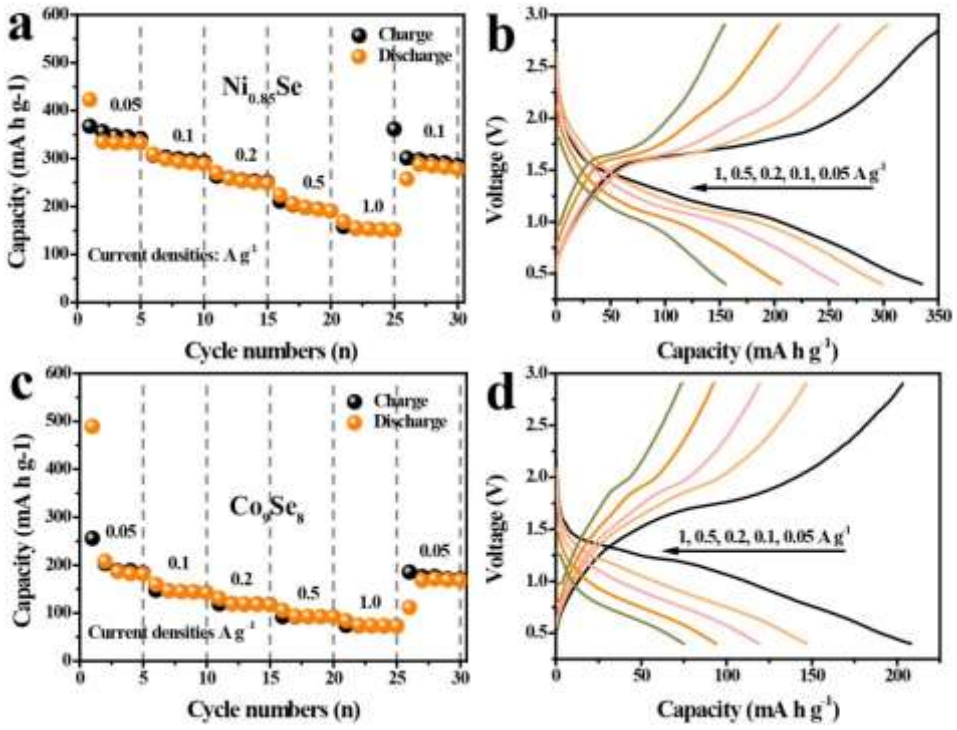

Fig. S9. Rate performance of $Ni_{0.85}Se$ and Co_9Se_8.

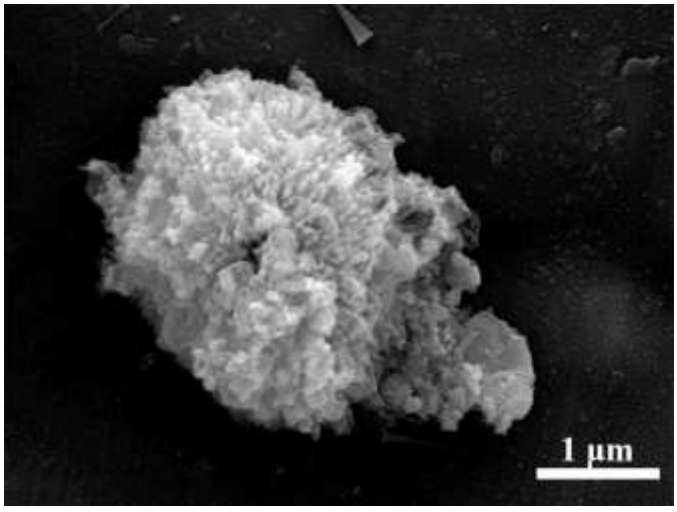

Fig. S10. FESEM image of $NiCo_2Se_4$ after circulation.

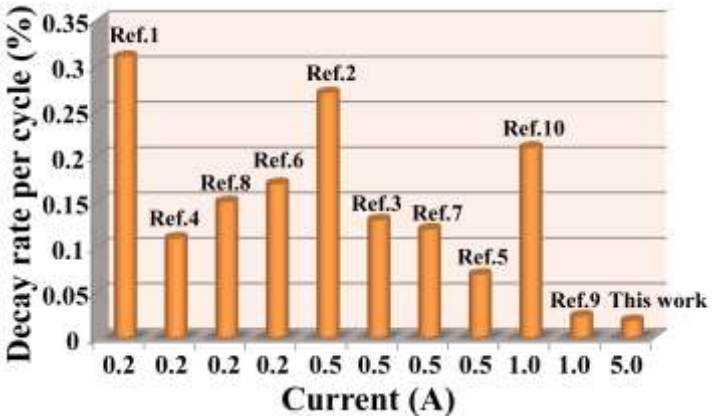

Fig. S11. Comparisons of the decay rate per cycle with other works.

Table 1. Summary for the cycle life of the representative selenide-based anode materials for SIBs.

Materials	Current density (mA g^{-1})	Cycles	Capacity (mAh g^{-1})	Capacity decay rate per cycle(%)	Ref.
$NiCo_2Se_4$	**5000**	**2500**	**230**	**0.019%**	**This work**
$(NiCo)/CoSe_2$	200	80	497	0.31%	1-2017
$Ni_{1.5}CoSe_5$	500	80	360	0.27%	2-2018
$Ni_{1.8}Co_{1.2}Se_4$	500	100	379.3	0.13%	3-2018
$C@Ni_xCo_{1-x}Se_2$/CNF	200	100	499	0.11%	4-2017
$NiCoSe_2$@C	500	250	338.3	0.07%	5-2019
CNT-$CoSe_2$@NC	200	120	404	0.17%	6-2019
CoSe/NC-L	500	150	397	0.12%	7-2019
$CoSe_2$@NC	200	100	555	0.15%	8-2018
$Co_{0.85}Se$ NSs@rGO	1000	800	382	0.024%	9-2018
$NiSe_2$/NC	1000	150	308	0.21%	10-2018

Table 2. Kinetic parameters of $NiCo_2Se_4$, $Ni_{0.85}Se$ and Co_9Se_8 obtained from equivalent circuit fitting.

Anode material	Rct (Ω)
$NiCo_2Se_4$	26.46
$Ni_{0.85}Se$	40.13
Co_9Se_8	43.54

Table 3. The D_{Na+} values for the electrochemistry processes of $NiCo_2Se_4$, $Ni_{0.85}Se$ and Co_9Se_8.

Anode material	Diffusion coefficient ($cm^2\ s^{-1}$)
$NiCo_2Se_4$	4.22×10^{-12}
$Ni_{0.85}Se$	1.77×10^{-13}
Co_9Se_8	9.63×10^{-13}

References

1 S.-K. Park, J. K. Kim, Y. C. Kang, Metal–organic framework-derived $CoSe_2$/$(NiCo)Se_2$ box-in-box hollow nanocubes with enhanced electrochemical properties for sodium-ion storage and hydrogen evolution, *J. Mater. Chem. A*, 2017, **5**, 18823-18830.

2 Y.-Y. Wang, H. Fan, B.-H. Hou, X.-H. Rui, Q.-L. Ning, Z. Cui, J.-Z. Guo, Y. Yang, X.-L. Wu, $Ni_{1.5}CoSe_5$ nanocubes embedded in 3D dual N-doped carbon network

as advanced anode material in sodium-ion full cells with superior low-temperature and high-power properties, *J. Mate. Chem. A*, 2018, **6**, 22966-22975.

3 B.-H. Hou, Y.-Y. Wang, D.-S. Liu, Z.-Y. Gu, X. Feng, H. Fan, T. Zhang, C. Lü, X.-L. Wu, N-Doped Carbon-Coated $Ni_{1.8}Co_{1.2}Se_4$ Nanoaggregates encapsulated in N-doped carbon nanoboxes as advanced anode with outstanding high-rate and low-temperature performance for sodium-ion half/full batteries, *Adv. Funct. Mater.*, 2018, **28**, 1805444.

4 C. Wu, Y. Wei, Q. Lian, C. Cui, W. Wei, L. Chen, C. Li, Intrinsic conductivity optimization of bi-metallic nickel cobalt selenides toward superior-rate Na-ion storage, *Mater. Chem. Front.*, 2017, **1**, 2656-2663.

5 M. Jia, Y. Jin, P. Zhao, C. Zhao, M. Jia, L. Wang, X. He, Hollow $NiCoSe_2$ microspheres@N-doped carbon as high-performance pseudocapacitive anode materials for sodium ion batteries, *Electrochim. Acta*, 2019, **310**, 230-239.

6 S. H. Yang, S.-K. Park, Y. C. Kang, Mesoporous $CoSe_2$ nanoclusters threaded with nitrogen-doped carbon nanotubes for high-performance sodium-ion battery anodes, *Chem. Eng. J.*, 2019, **370**, 1008-1018.

7 X. Li, W. Zhang, Y. Feng, W. Li, P. Peng, J. Yao, M. Li, C. Jiang, Ultrafine CoSe nano-crystallites confined in leaf-like N-doped carbon for long-cyclic and fast sodium ion storage, *Electrochim. Acta*, 2019, **294**, 173-182.

8 S.-K. Park, Y. C. Kang, MOF-templated N-doped carbon-coated $CoSe_2$ nanorods supported on porous CNT microspheres with excellent sodium-ion storage and electrocatalytic properties, *ACS Appl. Mater. Interfaces*, 2018, **10**, 17203-17213.

9 Y. Huang, Z. Wang, Y. Jiang, S. Li, Z. Li, H. Zhang, F. Wu, M. Xie, L. Li, R. Chen, Hierarchical porous $Co_{0.85}Se$@reduced graphene oxide ultrathin nanosheets with vacancy-enhanced kinetics as superior anodes for sodium-ion batteries, *Nano Energy*, 2018, **53**, 524-535.

10 S.Liu, D. Li, G. Zhang, D. Sun, J. Zhou, H. Song, Two-dimensional $NiSe_2$/N-rich carbon nanocomposites derived from Ni-hexamine frameworks for superb Na-ion storage, *ACS Appl. Mater. Interfaces*, 2018, **10**, 34193-34201.